SOLAR-ELECTROCATALYTIC PRODUCTION OF H_2 AND S FROM TOXIC H_2S BY $In_2S_3/AgIO_3$ PHOTOANODE COUPLED I^-/I_3^- CYCLIC REDOX SYSTEM

Akeem Adeyemi Oladipo[1], Roozbeh Vaziri[1], Ayodeji Olugbenga Ifebajo[2]

[1]Faculty of Engineering, Cyprus Science University, Girne, North Cyprus via Mersin 10 Tukey
[2]Chemistry Department, Faculty of Arts and Science, Eastern Mediterranean University, Famagusta, North Cyprus via Mersin 10 Tukey

Corresponding author: AA Oladipo, e-mail: akeem.oladipo@kiu.edu.tr

REFERENCE NO

HYPR-05

Keywords:
H_2S splitting
Solar-electrocatalytic system
Hydrogen production
$In_2S_3/AgIO_3$ photoanode
I^-/I_3^- Cyclic redox

ABSTRACT

A solar responsive electrocatalytic cell (SEC) system comprising a heterostructured $In_2S_3/AgIO_3$ photoanode and Pt/C–based waterproofed carbon fibre cathode was facilely constructed for the recovery of H_2 and S from toxic H_2S in a cyclic redox system of I^-/I_3^-. The H_2S was oxidized to S by I_3^- in the photoanode compartment and H^+ was efficiently reduced to H_2 in the photocathode region. A maximum H_2 and S production rate of ~0.26 mmol h^{-1} cm^{-2} and ~0.23 mmol h^{-1} cm^{-1} were achieved and the photocurrent density of ~0.9 mA cm^{-2} was attained during the entire operation. significantly increased by 128%. The $In_2S_3/AgIO_3$ photoanode exhibited high energy conversion efficiency and polysulfides were not detected after the reaction, suggesting that the toxic H_2S was completely converted into H_2 and S. The proposed system with I^-/I_3^- redox provides an energy-sustaining method for simultaneous treatment of toxic H_2S and clean fuel production.

1. INTRODUCTION

Hydrogen sulphide, H_2S, is an acutely corrosive, flammable and toxic gas generated from various industries. The H_2S remains a disposable gaseous species due to its environmental hazardous nature. However, the abundant availability of H_2S in many industrial and natural resources [1] and its low thermodynamic decomposition (ΔG^o=33.2 $kJmol^{-1}$) [2, 3], makes it a viable economic raw source for the production of environmentally clean fuel, H_2 [1–4].

Considering the increasing energy and environmental pollution crisis, the decomposition of H_2S is obviously necessary for sustainable aesthetic environmental abatement and hydrogen production. Various methods have been reported for the decomposition of H_2S, including the thermal, photochemical, plasma and electrochemical decomposition [5,6]. Different degrees of success have been recorded by the existing methods, however, they still suffer from several shortcomings. For instance, plasma technique requires a complex equipment [5], and the electrochemical methods require an external source of energy [2].

Recently, the solar-electrocatalytic technique has attracted wide attention because it provides a solar energy driven pathway to degrading pollutants, generating electricity and producing hydrogen [7–10]. Particularly, the photoelectrocatalytic (PEC) system is a cost-effective and sustainable technology to simultaneously treat H_2S polluted water and recover H_2 and S. Highly stable photoelectrode materials with high photoconversion efficiency and high resistant to photocorrosion are required to realize the PEC treating H_2S in practice [10].

In the traditional photoelectrocatalytic (PEC) and photocatalytic systems, the S^{2-} can be easily oxidized to polysulfide (S_y^{n-}) by the photogenerated radicals, resulting in secondary pollution [10]. Also, the traditional PEC system requires an external bias to promote electrochemical decomposition and facilitate the photocatalysis [2, 6].

Considering the shortcomings of the traditional PEC system, herein, we propose a self-bias solar responsive electrocatalytic fuel cell (SEC) coupled with I^-/I_3^- cyclic redox system to accelerate the decomposition of H_2S, and uniquely produce elemental sulphur (S).

In recent years, a growing number of silver-based oxy-acid salts photocatalysts have been extensively investigated [11, 12] for the degradation of environmental pollutants. Among them, $AgIO_3$ has attracted a wide attention due to the lone pair electrons of I^{5+} in $(IO_3)^-$ anion [11], thus beneficial to form layered crystal structure with an internal self-built electric field, which could improve the charge separation efficiency [12]. Unfortunately, the relatively large empirical band gap (~3.4 eV) of $AgIO_3$ limits its photoabsorption to a narrow region leading to its sluggish reaction to visible light [11, 12]. Numerous efforts have been directed to produce materials with high photo-stability and activity under visible light illumination since ~45% of the earth solar energy is made up of visible light [11–13].

On the contrary, In_2S_3 is a III–VI group *n*–type semiconductor with a narrow band gap of ~2.0 eV [14] and potential candidate for photocatalytic applications. To upgrade the $AgIO_3$ response to visible light and restrict its electron-holes recombination rate, it is exceptionally attractive to couple In_2S_3 and $AgIO_3$ to build high-efficiency heterojunctions with increased visible light induced and photocatalytic activity.

For the first time, we proposed a solar-electrocatalytic (SEC) system using a new $In_2S_3/AgIO_3$ photoanode and a cyclic I^-/I_3^- redox reaction for splitting toxic H_2S into H and S. The $In_2S_3/AgIO_3$ photoanode was synthesized via a controllable, simple and scalable chemical deposition technique. The physio-chemical and photoelectrochemical properties of the obtained $In_2S_3/AgIO_3$ are reported. The efficiency of the proposed SEC system for elemental S recovery and hydrogen generation was examined. The H_2S was uniquely oxidized into S (E^o S/H_2S = 0.14 V vs NHE) by the I_3^- (E^o (I_3^-/I^-) = 0.54 vs NHE) generated in the photoanode compartment of the system. A Pt/C-based air-breathing electrocatalyst was used as the photocathode, the H^+ was efficiently reduced into H_2 in the cathode region.

Overall, the results showed that $In_2S_3/AgIO_3$ heterojunction displayed better photoelectrocatalytic activity than pristine materials. Furthermore, the self-bias SEC-H_2S system exhibited relatively higher recovery rates of H_2 and S and stability in a long-term operation than most reported systems.

2. EXPERIMENTAL SECTION

2.1. Electrode preparation

Analytically pure chemical reagents were used and supplied by Sigma-Aldrich (UK). Aqueous solutions were freshly prepared using high-purity deionized water. Fluorine-doped tin oxide (FTO) coated glass slide (~7 Ω/cm^{-1}) purchased from Sinopharm Chemical Reagent Co., Ltd. Carbon fibre was purchased from Shanghai Hesen Electric Co. Ltd., China.

$In_2S_3/AgIO_3$ photoanode was prepared by a two-step process of chemical bath deposition followed by calcination. The $AgIO_3$ precursor solution was prepared as we previously reported [11]. The FTO glass (~7 Ω/cm^{-1}) was dipped into the $AgIO_3$ precursor solution and the mixtures were heated to 90 ^oC for 30 min in a temperature-controlled bath (heating rate of 5 °C/min). The as-prepared sample was cooled to ambient temperature, rinsed with deionized water, dried and calcined at 650 °C for 1 h.
Then, FTO glass (10 × 60 × 1 mm^3) containing the prepared $AgIO_3$ nanoparticle was immersed in 50 mL of $InCl_3$ (0.15 M) solution for 20 min. Then, 70 mL of Na_2S (0.2 M) was added dropwise to the solution. After 2 h of reaction, the $In_2S_3/AgIO_3$ photoanode was slightly rinsed with ethyl

alcohol, immersed in distilled water for 10 min, and then dried in an oven at 70 ^{o}C for 1 h.

The Pt/C–based waterproof carbon fibre cathode was prepared via a slightly modified procedure [15]. Firstly, the carbon fibre was soaked in acetone for 1 h to remove organic impurities and severally washed with distilled water, and dried in convectional oven at 80 ^{o}C for 3 h. Then, the dried carbon fibre was waterproofed with two layers of 50% poly-tetrafluoroethylene on both sides [16].

150 mg commercial Pt/C electrocatalyst (29% Pt) was immersed in 100 mL aqueous solution of 120 mL 7% Nafion (as catalyst binder) and 60 ml isopropyl alcohol, then 10 mL surfactant (Triton X100, 6.5%) was added to form a pulp-like homogeneous paste. The catalytic homogeneous paste was uniformly casted onto the waterproofed carbon fibre and dried for 48 h at ambient temperature. The quantity of Pt contained in the as-prepared cathode was 12.9 wt% (0.25 mg cm^{-2}) as determined by ICP–MS.

2.2. Characterizations

The morphology and chemical compositions of the samples were examined by scanning electron microscopy equipped with energy dispersive X-ray spectroscopy (SEM–EDX; JSM-IT500HR, Jeol, Japan). Optical absorption measurements were recorded with GENESYS 10S UV-Vis spectrophotometer (Thermofisher, USA) in a spectrum range of 200–800 nm. The samples crystallographic data were obtained with X-ray diffractometer (XRD; D8 Advance, Bruker, Germany) at a scan rate of 5^{o}/min. The photoresponse measurements of the $In_2S_3/AgIO_3$ photoanode were carried using in standard a three-electrode system on an electrochemical workstation (CHI 600E, CH Instruments, Inc. USA) with the Pt foil as the auxiliary electrode and Ag/AgCl electrode as the reference electrode.

2.3. Solar-electrocatalytic cell set-up for H_2S splitting

In this research, a self-driven H-shape double chamber solar-electrocatalytic cell (SEC) was utilized for H_2S splitting. The fabricated reactor consists of a proton-exchange membrane and a specialized accessory for S collection. The $In_2S_3/AgIO_3$ (effective area of 4.5 cm^2) was fixed into the anodic region with an electrode holder and 70 mL of 0.25M Na_2SO_4 containing 0.1−0.5M KI as the electrolyte. The cathodic region contained the cathode (effective area of 6.5 cm^2) and 70 mL of 0.25 M Na_2SO_4 was used as the electrolyte.

To eliminate the air before the operation, nitrogen gas was introduced into the SEC reactor for 15 min. Under simulated sunlight illumination, H_2S gas was periodically pumped into the anodic compartment, followed by filtration through the customized S collection accessory. The filtered solution was reintroduced into the anodic segment. The H_2 gas production rate and stability were monitored using Agilent 6890 gas chromatograph (Agilent, USA).

3. RESULTS AND DISCUSSION

3.1. Characterization of the photoelectrodes

The photoelectrodes utilized to construct the self-driven SEC system were characterized as shown in Fig.1–2. In Fig.1a, the X-ray diffractogram shows that the samples exhibit highly crystalline nature, with sharp and intense peaks. The pure $AgIO_3$ shows characteristic diffraction peaks of (021), (210), (041), (211), (230), (002), (231), (061), (212), (232) and (271) which closely matched well with the orthorhombic $AgIO_3$ (JCPDS card no. 71-1928) [11]. Also, it can be seen that pure In_2S_3 exhibits the distinctive diffraction peaks of (008), (109), (206), (208) and (2212) at 2θ values of 25.7°, 28.7°, 31.6°, 34.3° and 49.2°, respectively. These peaks matched well with the tetragonal In_2S_3 (JCPDS card no. 25-0390) [17]. For $In_2S_3/AgIO_3$ composite, the XRD patterns exhibit diffraction peaks corresponding to

In_2S_3 and $AgIO_3$ phases, indicating that the pristine materials were well coupled and $In_2S_3/AgIO_3$ was synthesized successfully.

The photoelectrochemical behaviour of the pure In_2S_3, $AgIO_3$ and $In_2S_3/AgIO_3$ composite with a cut-off filter is shown in Fig. 1b. All the samples exhibit relatively reversible and stable photoresponses at light-on and light-off under visible-light irradiation. Obviously, the $In_2S_3/AgIO_3$ exhibited the highest photocurrent approximately 8.0 μA cm^{-2} compared to that of $AgIO_3$ and In_2S_3 (4.8 and 2.2 μA cm^{-2}), indicating a more efficient separation of the photoexcited electron–hole pairs as compared with the pure materials [11, 14, 17].

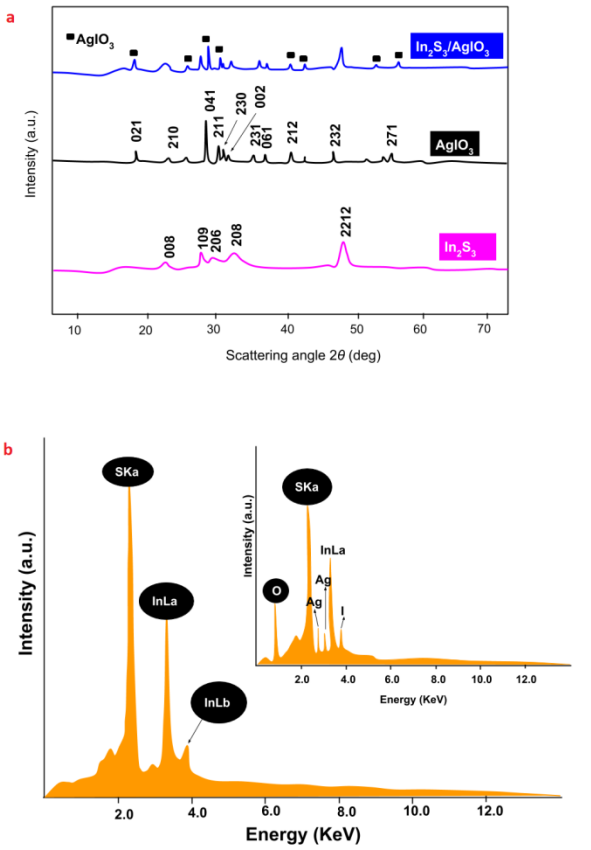

Fig. 1. (a) XRD (b) photocurrent response (c) SEM images (d) EDX of the samples

The photoelectrochemical behaviour of the pure In_2S_3, $AgIO_3$ and $In_2S_3/AgIO_3$ composite with a cut-off filter is shown in Fig. 1b. All the samples exhibit relatively reversible and stable photoresponses at light-on and light-off under visible-light irradiation. Obviously, the $In_2S_3/AgIO_3$ exhibited the highest photocurrent approximately 8.0 μA cm^{-2} compared to that of $AgIO_3$ and In_2S_3 (4.8 and 2.2 μA cm^{-2}), indicating a more efficient separation of the photoexcited electron–hole pairs as compared with the pure materials [11, 14, 17].

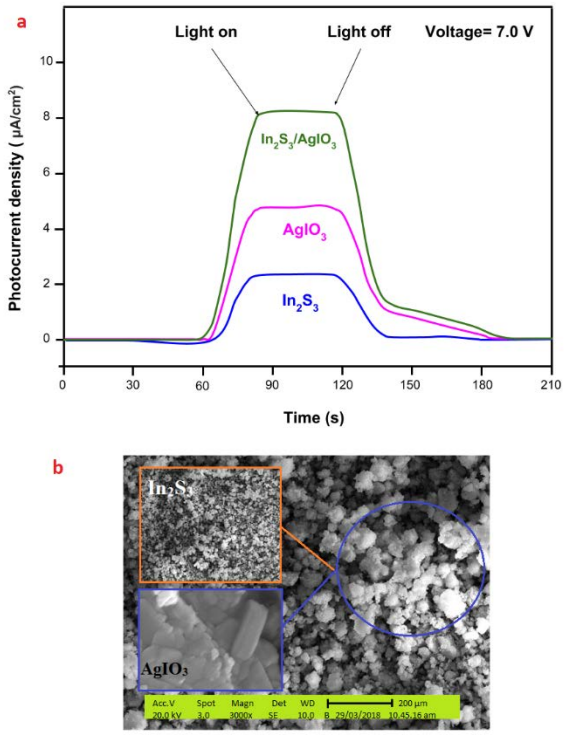

Fig. 2. (a) EDX (b) SEM images of the samples (insert: In_2S_3 (up) and $AgIO_3$ (down))

The elemental composition obtained by the EDX indicates the presence of In and S in the pure In_2S_3 (Fig.2a). The EDX spectrum clearly showed that the $In_2S_3/AgIO_3$ composite (insert) was composed of indium, iodine, sulphur, oxygen and silver elements. The atomic percentage of indium (26.5%), oxygen (23.9%), sulphur (10.6%), silver (26.5%) and iodine (12.5%) suggested the presence of In_2S_3 and $AgIO_3$ in the composite ($In_2S_3/AgIO_3$). The morphology of samples is shown in Fig.2b. The $AgIO_3$ micrograph displayed an irregular rod-like structure with smooth and clean surfaces. The average length

and width of the $AgIO_3$ microcrystal are about 0.6–1.7 μm. The pure In_2S_3 is composed of flake-like nanoparticles in the range of several micrometres. After the incorporation of In_2S_3, the rod-like morphology of the $AgIO_3$ (insert) was altered to a quake-like morphology and the $In_2S_3/AgIO_3$ exhibits interesting coarse morphology which could favour the photoelectrocatalytic reactions. On the basis of the theory of light absorption for $In_2S_3/AgIO_3$, it is proverbial to calculate the band gap energy through the Kubelka–Munk theory [14, 15, 18]:

$$A(hv - E_g)^{n/2} = ahv \quad (1)$$

Where E_g, h, A, v and a are optical band gap energy, Plank constant, constant, optical frequency and absorption coefficient determined by scattering and reflectance spectra. The estimated E_g values of In_2S_3 and $AgIO_3$ are 2.85 eV and 3.35 eV, respectively. The conduction band offset (E_c) and valence band (E_v) of the samples were calculated using the empirical formula described in our earlier report [19]. After the integration of the individual component, the $In_2S_3/AgIO_3$ heterojunction displayed mixed properties of pure In_2S_3 and $AgIO_3$ with an absorption edge around 470 nm associated with a corresponding band gap of 2.64 eV.

3.2. SEC operating mechanism for H_2S splitting

The self-driven SEC was achieved due to matched Fermi levels between the $In_2S_3/AgIO_3$ and Pt/C–based photocathode, which accounts for the generation of photovoltage in the SEC system. The photoelectrochemical behaviour of the as-fabricated Pt/C cathode herein is relatively comparable to those reported by Huang et al. (2015) and Xiong et al. (2016).

The Fermi level of Pt/C is less negative than that of $In_2S_3/AgIO_3$ (0.7 V vs NHE vs 0.4 V vs NHE) so the electrons generated from $In_2S_3/AgIO_3$ and the holes from Pt/C combined with each other by an interior bias through the external circuit. Also, the h^+ of the photoanode and the e^- of the photocathode are released to produce redox reactions in the solution. Hence, this high self-bias process reduced the fast combination of the photogenerated electron−hole pairs during the operation [2].

Both electrodes were simultaneously illuminated by simulated sunlight, and H_2S gas was pumped into the anodic chamber while elemental S was collected via an external duct. During operation, the photogenerated holes (h^+) and hydroxyl radicals from the $In_2S_3/AgIO_3$ first oxidized the I^- to I_3^-, then the generated I_3^- selectively converts the H_2S into H^+ and elemental S and finally reduced to I^- in the anodic region. The H^+ moved to the cathodic chamber where the photogenerated electrons (e^-) from Pt/C reduced it to generate H_2 as shown in Fig.3. Overall, with the connected redox couples (I^-/I_3^-), the photogenerated e^- and h^+ make H_2S splitting and energy recovery possible via solar energy as summarized in Eqs. 2–7.

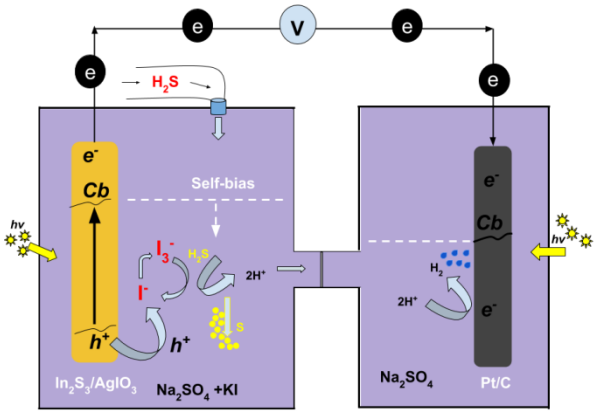

Fig. 3. Schematic mechanism of the self-bias SEC-H_2S splitting system

Anode chamber:

$$In_2S_3/AgIO_3 + hv \rightarrow h^+ + e^- \quad (2)$$

$$3I^- + 2h^+ \rightarrow I_3^- \quad (3)$$

$$I_3^- + H_2S \rightarrow 2H^+ + S\downarrow + 3I^- \quad (4)$$

Cathode chamber:

$$Pt/C + hv \rightarrow h^+ + e^- \quad (5)$$

$$2H^+ + e^- \rightarrow H_2\uparrow \quad (6)$$

Overall reaction: $H_2S \rightarrow H_2 \uparrow + S \downarrow$ (7)

3.2.1. Effect of electrolyte in the SEC-H_2S system

The photoelectric properties of the proposed SEC-H_2S system were investigated and optimized under different concentrations of KI and Na_2SO_4. First, the accumulation and consumption of KI are examined and discussed. The percentages of I^-/I_3^- ions during the operation in 70 mL of 0.25 M Na_2SO_4 is depicted in Fig.4. As depicted, the concentration of I_3^- ion increased steadily and I^- was simultaneously consumed within the first 70 min of operation. After the introduction of the toxic H_2S into the anodic chamber, the generated I_3^- selectively reacted with H_2S to produce S and reduced to I^-. Afterwards, the redox system ran into the second cycle until the percentage ratio between I^- and I_3^- reached a dynamic equilibrium (Fig.4a).

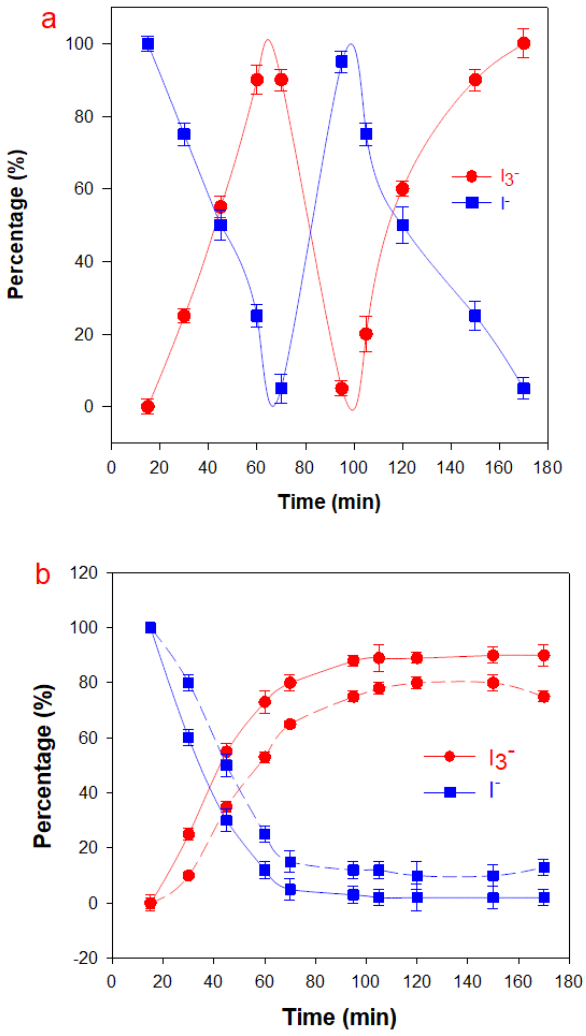

Fig. 4. (a) Accumulation and consumption of I^- and I_3^- during the operation (b) Percentage of I^-/I_3^- in the presence of scavenger during the first cycle (*continuous line*: the presence of t-butyl alcohol and *dashed line*: the presence of EDTA)

To investigate the main active photogenerated species responsible for the catalytic reaction, contrast, two different radical scavengers EDTA and t-butyl alcohol were added to the anodic chamber of the SEC system to trap photogenerated holes (h^+) and hydroxyl radicals (OH·), respectively. As indicated in Fig.4b, the I_3^- formation rate was slightly reduced with the existence of t-butyl alcohol. However, the EDTA remarkably suppressed the formation rate of I_3^-, and thus implied that the holes (h^+) h+ is the dominant active species and played a significant role during the photoelectrocatalytic reaction as summarized in Eqs. 2–4. Similar observations have been reported elsewhere [2, 11, 19].

3.2.2. Photohydrogen and S production rates

To investigate the performance of the SEC-H_2S system, elemental sulphur and hydrogen gas were continuously collected during 10 h operation. Fig.5 shows the production rate of H_2 and elemental S by the SEC-H_2S system. The production rates of H_2 were maintained at ~0.026 mmol $h^{-1}cm^{-2}$ when 0.15M KI was introduced into the system. As the concentration of the KI increases, the H_2 production also increased, however, no significant increment was recorded beyond 0.2 M KI. As noted, the hydrogen production rates increased slightly in the presence of 0.1M KI in the first 4 h, meanwhile, a decreasing trend was noticed beyond the 6th hour of operation. It is worth mentioning that, the concentration of KI influenced the bias potential between the photoanode and photocathode [22]. Hence, a higher concentration of I^- would lead to higher hydrogen production and photocurrent density [2, 22].

Similarly, in the presence of 0.15M KI, the S production rate was maintained at ~0.027 mmol $h^{-1}cm^{-2}$ suggesting that H_2S was completely converted into H_2 and S. As indicated in Fig.5b, with 0.15M KI and 0.2M H_2S, the productivity of S was ~0.018 M, indicating that S was absolutely generated by I_3^-. This result also explained that the oxidation of H_2S by I_3^- at 0.2M KI concentration 0.1M is much faster than in the presence of 0.25M KI. A control experiment was performed in the absence of the I^-/I_3^- redox cycle in the anodic chamber to investigate the formation of polysulfide. After 2h of operation, a turbid yellow-like solution was obtained which is the typical feature of polysulfide solutions. The result herein, confirmed that the H_2S was completely converted into H_2 and S in the presence the of I^-/I_3^-.

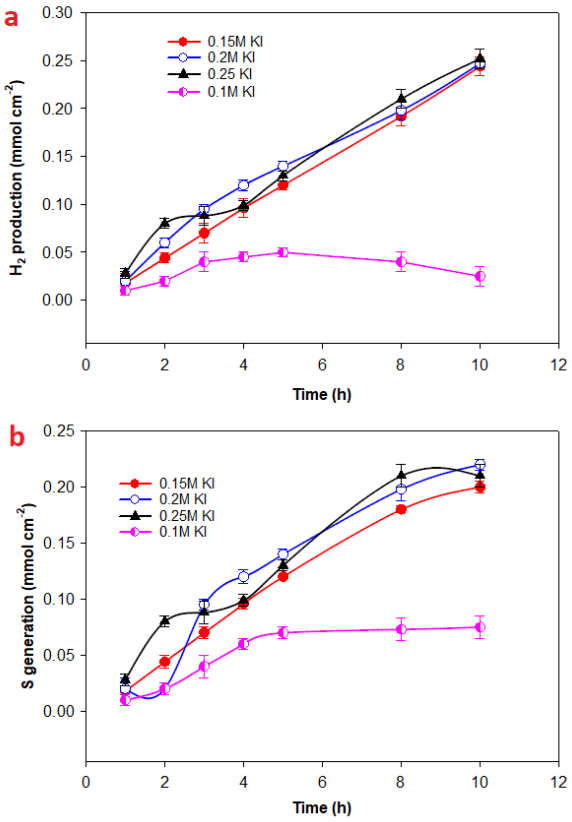

Fig. 5. (a) Hydrogen production (b) S generation in the presence of different concentration of KI

During the operation, the photocurrent density of the system was measured and the output power density (P) of the SEC-H_2S system was calculated using the following formula:

$$P = I_{sc}V_{oc} \times F_f \qquad (8)$$

Here, P is the maximum power density, I_{sc} is the short-circuit current density, F_f is the fill factor of the system and V_{oc} is the open-circuit voltage. As shown in Fig.6, the photocurrent density was approximately 0.89 mA cm^{-2} at the initial stage. The colour of the solution in the anode compartment gradually changed from transparent to fair yellow and finally to light red suggesting the formation of I_3^-. Meanwhile, H_2 bubbles were noticed in the cathode chamber. A certain quantity of H_2S was then pumped into the anodic cell, as expected, the photocurrent density sharply reduced to 0.17 mA cm^{-2} and the light red solution turned to a milky white turbid

solution. At the end of each cycle, the solid S product was separated via a specialized circulation duct system. ~0.23 mW cm^{-2} was obtained as the maximum output power density of the SEC system was and the light energy conversion efficiency was 0.75%. Conclusively, the results demonstrated that the photocurrent and the open-circuit potential could reach ~0.9 $mAcm^{-2}$ and 0.45 V, respectively. Hence, the self-bias SEC-H_2S system is suitable for green energy generation and elimination of toxic gases.

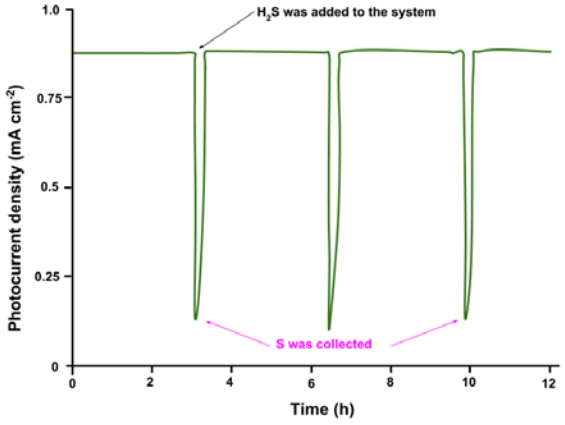

Fig. 6. Variation in the photocurrent during the SEC-H_2S system operation

4. CONCLUSIONS

In summary, we investigated the efficiency of a new $In_2S_3/AgIO_3$ photoanode and Pt/C photocathode in a self-driven photoelectrocatalytic system for decomposing toxic H_2S into clean hydrogen fuel and S with simultaneous green electricity production. With the connected redox couples (I^-/I_3^-), the photogenerated holes of the $In_2S_3/AgIO_3$ anode and electrons of the photocathode made the H_2S splitting and energy recovery feasible via solar energy. High recovery rates for H_2 and S were obtained up to ~0.26 mmol h^{-1} cm^{-2} and ~0.23 mmol h^{-1} cm^{-1}, respectively. Also, the photocurrent was maintained at ~0.9 mA cm^{-2} during the 10 h operation.

Acknowledgements
The authors acknowledged the support provided by electrical engineering of CSU and polymeric materials research lab of Prof. Mustafa Gazi of Chemistry Department, Eastern Mediterranean University.

References

[1] Guldal NO, Figen HE, Baykara SZ, Perovskite catalysts for hydrogen production from hydrogen sulphide, *Int J Hydrogen Energy* 43, 2018, 1038–46.

[2] Luo T, Bai J, Li J, Zeng Q, Ji Y, Qiao L, Li X, Zhou B, Self-driven photoelectrochemical splitting of H_2S for S and H_2 recovery and simultaneous electricity generation, *Environ Sci Technol* 51, 2017, 12965–71.

[3] Subramanian E, Baeg JO, Lee SM, Moon SJ, Kong KJ, Dissociation of H_2S under visible light irradiation (λ ≥420 nm) with $FeGaO_3$ photocatalysts for the production of hydrogen, *Int J Hydrogen Energy* 33, 2008, 6586–94.

[4] Guldal NO, Figen HE, Baykara SZ, New catalysts for hydrogen production from H_2S: preliminary results, *Int J Hydrogen Energy* 40, 2015, 7452–8.

[5] Nunnally T, Gutsol K, Rabinovich A, Fridman A, Gutsol A, Plasma dissociation of H_2S with O_2 addition, *Int J Hydrogen Energy* 39, 2014, 12480–89.

[6] Reverberi AP, Klemes JJ, Varbanov PS, Fabiano B, A review on hydrogen production from hydrogen sulphide by chemical and photochemical methods, *J Clean Prod* 136, 2016, 72–80.

[7] Angela AT, Didier R, Nicolas K, A parametric study of the UV-A photocatalytic oxidation of H_2S over TiO_2, *Appl Catal B* 115, 2012, 209–218.

[8] Bai J, Li J, Liu Y, Zhou B, Cai W, A new glass substrate photoelectrocatalytic electrode for efficient visible-light hydrogen production: CdS sensitized TiO_2

nanotube arrays, *Appl Catal B* 95, 2010, 408–413.

[9] Thabet M, El-Zomrawy AA, Degradation of acid red 17 dye with ammonium persulphate in acidic solution using photoelectrocatalytic methods, *Arabian J Chem* 9, 2016, S204–S208.

[10] Lianos P, Review of recent trends in photoelectrocatalytic conversion of solar energy to electricity and hydrogen, *Appl Catal B* 210, 2017, 235–254.

[11] Oladipo AA, Vaziri R, Abureesh MA, Highly robust $AgIO_3$/MIL-53 (Fe) nanohybrid composites for degradation of organophosphorus pesticides in single and binary systems: Application of artificial neural networks modelling, *J Taiwan Instit Chem Eng* 83, 2018, 133–142.

[12] Xie J, Cao Y, Jia D, Li Y, Wang K, Xu H, In situ solid-state fabrication of hybrid AgCl/AgI/$AgIO_3$ with improved UV-to-visible photocatalytic performance, *Sci Reports* 7, 2017, 12365.

[13] Gazi M, Oladipo AA, Ojoro ZE, Gulcan HO, High-performance nanocatalyst for adsorptive and photo-assisted Fenton-like degradation of phenol: modeling using artificial neural networks, *Chem Eng Comm* 204, 2017, 729–38.

[14] Yan T, Wu T, Zhang Y, et al., Fabrication of In_2S_3/Zn_2GeO_4 composite photocatalyst for degradation of acetaminophen under visible light, *J Colloid Interf Sci* 506, 2017, 197–206.

[15] Xie S, Ouyang K, Shao Y, A solar responsive photocatalytic fuel cell with a heterostructured $ZnFe_2O_4$/TiO_2-NTs photoanode and an air-breathing cathode, *Int J Hydrogen Energy* 42, 2017, 29201–29209.

[16] Cheng S, Liu Hong, Logan BE, Increased performance of single-chamber microbial fuel cells using an improved cathode structure, *Elecetrochem Commun* 8, 2006, 489–494.

[17] Zhang X, Li X, Shao C, Li J, Zhang M, Zhang P, Wang K, Lu N, Liu Y, One-dimensional hierarchical heterostructures of In_2S_3 nanosheets on electrospun TiO_2 nanofibers with enhanced visible photocatalytic activity, *J Hazard Mater* 260, 2013, 892–900.

[18] Cao QW, Zheng YF, Song XC, Enhanced visible-light-driven photocatalytic degradation of RhB by $AgIO_3$/WO_3 composites, *J Taiwan Inst Chem Eng* 70, 2017,359–365.

[19] Oladipo AA, MIL-53 (Fe)-based photo-sensitive composite for degradation of organochlorinated herbicide and enhanced reduction of Cr(VI), *Proc Saf Environ Prot* 116, 2018, 413–423.

[20] Xiong Z, Liao S, Hou S et al., Construction of a high-performance air-breathing cathode using platinum catalyst supported by carbon black and carbon nanotubes, *Int J Hydrogen Energy* 41, 2016, 9191–9196.

[21] Huang C, Odetola CB, Rodgers M, Nanoparticle seeded pulse electrodeposition for preparing high performance Pt/C electrocatalysts, *App Catal A* 499, 2015, 55–65.

[22] Zhu H, Hagfeldt AA, Boschloo G, Photoelectrochemistry of Mesoporous NiO Electrodes in Iodide/Triiodide Electrolytes, *J Phys Chem C* 111, 2007, 17455−17458.